Biosensors and Bioelectronics 124–125 (2019) 184–190

Contents lists available at ScienceDirect

Biosensors and Bioelectronics

journal homepage: www.elsevier.com/locate/bios

Ti_3C_2 MXenes nanosheets catalyzed highly efficient electrogenerated chemiluminescence biosensor for the detection of exosomes

Huixin Zhang[a,b], Zonghua Wang[a,*], Qiuxia Zhang[b], Feng Wang[b], Yang Liu[b,*]

[a] Shandong Sino-Japanese Center for Collaborative Research of Carbon Nanomaterials, College of Chemistry and Chemical Engineering, Qingdao University, Qingdao, Shandong 266071, China

[b] Department of Chemistry, Beijing Key Laboratory for Analytical Methods and Instrumentation, Kay Lab of Bioorganic Phosphorus Chemistry and Chemical Biology of Ministry of Education, Tsinghua University, Beijing 100084, China

ARTICLE INFO

Keywords:
Exosomes
Ti_3C_2 MXenes
Nanoprobe
Electrogenerated chemiluminescence
Biosensor

ABSTRACT

Exosomes have been reported to play an important role in the anti-tumor immune response, tumor diagnosis and other processes, and are promising biomarkers for early cancer diagnosis. In this work, a sensitive electrogenerated chemiluminescence (ECL) biosensor was developed for detection of exosomes using aptamer modified two-dimensional material Ti_3C_2 MXenes nanosheets as the ECL nanoprobe because of its large surface area, the excellent conductivity and catalytic properties. The exosomes can be high efficiently captured onto the electrode surface by an EpCAM protein recognized aptamer modified on the electrode surface. In addition, the ECL nanoprobe can also recognize the exosomes, and significantly enhanced the ECL signals of luminol. Based on this strategy, a highly sensitive ECL biosensor for MCF-7 exosomes detection was obtained. The detection limit is 125 particles μL^{-1}, which was over 100 times lower than that of conventional ELISA method. The as prepared ECL biosensor was performed successfully for MCF-7 exosomes detection in the serum. This strategy provided a feasible, sensitive and reliable tool for the exosomes detection in exosomes-related clinical diagnostics.

1. Introduction

Exosomes are nanoscale extracellular vesicles with sizes of 30–100 nm, which have received much attention in disease diagnosis due to their unique pathological and physiological significance (Chiu et al., 2016). Exosomes are found in most human bodily fluids including blood, urine, saliva, and breast milk (Raposo et al., 2013; Vlassov et al., 2012). They are secreted by most mammalian cells and carry factors promoting cell-cell communication, including mRNA, carbohydrates and protein (CD63, CD81, CD9 and EpCAM) (Mathivanan et al., 2010; Wang et al., 2017a, 2017b; Jiang et al., 2017), DNA (Nilsson et al., 2009; Valadi et al., 2007). Exosomes have been reported to play an important role in the anti-tumor immune response, tumor diagnosis and other processes, and are promising biomarkers for early cancer diagnosis. As a result, highly sensitive methods for exosomes detection are not only valuable to the clinic diagnostics but also important to provide deep insights regarding the fundamental biochemical process of tumor growth and metastasis.

Until now, various methods have been used for exosomes detection including western blot, flow cytometry (Liu et al., 2017a, 2017b), enzyme-linked immunosorbent (Ueda et al., 2014), colorimetric (Xia et al., 2017), Nanoparticle Tracking Analysis (NTA) (Dragovic et al., 2011; Gleadle et al., 2018; van der Pol et al., 2014), and tunable pore (Roberts et al., 2012). Although these methods are effective and powerful, they are still challenging in simplifying analysis procedures, reducing costs, and improving sensitivity for exosomes detection. Recently, electrochemical methods have become popular in the application of exosomes determination. For example, an electrochemical sensor based on microfabricated chip with multiplexed gold nanoparticles for exosomes detection has been developed, and an electrochemical aptasensor based on expanded nucleotide using DNA nanotetrahedra for exosomes detection has also been developed (Wang et al., 2017a; Wang et al., 2017b; Zhou et al., 2016). Although lots of efforts have been made in these years, simple, sensitive and reliable methods for the detection of exosomes are still a challenge.

Electrogenerated chemiluminescence (ECL), which involves a light emission process in a redox reaction of electrogenerated reactants, combines the electrochemical and luminescent techniques. Recently, ECL biosensor has been widely used in detection of proteins (Forzani et al., 2009; Li et al., 2004), DNA, enzymes (Zhang et al., 2014; Cheng et al., 2014; Dong et al., 2016a, 2016b; Liu et al., 2016), and clinical diagnosis, owing to its high sensitivity, rapidness, easy controllability

* Corresponding authors.
E-mail addresses: wangzonghua@qdu.edu.cn (Z. Wang), liu-yang@mail.tsinghua.edu.cn (Y. Liu).

https://doi.org/10.1016/j.bios.2018.10.016
Received 24 June 2018; Received in revised form 5 October 2018; Accepted 9 October 2018
Available online 12 October 2018
0956-5663/

and low cost (Feng et al., 2016; Zhang et al., 2013; Bertoncello et al., 2009). With the rapid development of nanomaterials, nanomaterials-based ECL biosensor (Lu et al., 2006; Chen et al., 2013) with superior performances have been continuously reported due to the excellent properties of nanomateirals, such as excellent conductivity, large surface area, good biocompatibility, and unique optical-electrochemical features and so on (Wang et al., 2013; Wang et al., 2014; Zhang et al., 2010; Ji et al., 2018a, 2018b; Wang et al., 2018a, 2018b; Ma et al., 2017). For example, a positive potential operation of a cathodic ECL biosensor based on luminol and graphene for cancer biomarker detection has been developed. An ECL biosensor using MoS_2 as basement showed improved sensitivity for cancer cell detection was also reported (He et al., 2015; Xu et al., 2011). The unique properties of the nanomaterial make it promising in the development of ECL biosensor with excellent performances.

In recent years, Ti_3C_2 MXenes, a new member of the multi-functional family 2D material (Naguib et al., 2011; Naguib et al., 2014) have been widely concerned, owing to its excellent properties such as good electrical conductivities, hydrophilic, large surfaces, easy film formation (Dong et al., 2018), and so on. Ti_3C_2 MXenes show great promise in numerous applications, such as catalysis (Seh et al., 2016; Zhang et al., 2016), biosensor (Wu et al., 2018), contaminant processing, supercapacitors (Naguib et al., 2012), lithium ion batteries (Liang et al., 2015; Dall et al., 2015). These good properties of Ti_3C_2 MXenes distinguish them from traditional 2D materials (Wang et al., 2018a, 2018b). Recently, Ti_3C_2 MXenes have been applied to the bioanalysis of small molecules such as dopamine, H_2O_2, and O_2, due to its great electron transfer ability, excellent catalytic ability and good biocompatibility (Lorencova et al., 2017; Fang et al., 2018; Lorencova et al., 2018). Moreover, the large surface area of Ti_3C_2 MXenes also allows it to be a good carrier to load more biomolecules, providing a significant magnification on the electrochemical sensing signals. Therefore, based on these unique features, such as excellent catalytic performance make Ti_3C_2 MXenes have great potential in fabrication of ECL biosensor with superior performances.

In this work, a sensitive ECL biosensor was fabricated for detection of exosomes using aptamer-modified Ti_3C_2 MXenes as ECL nanoprobe. The as-synthesized Ti_3C_2 MXenes nanosheets were serviced as a carrier to load more aptamer for exosomes recognition owing to its large surface area. An EpCAM protein recognized aptamer was modified on the electrode surface to capture exosomes with high efficiently, and then, the aptamer modified Ti_3C_2 MXenes to form nanoprobe can also recognize the exosomes. In addition, the excellent conductivity and catalytic properties of Ti_3C_2 MXenes nanosheets can also improve the electron transfer on the electrode interface and amplify the luminol ECL signal. As a result, the ECL signal of luminol can be significantly improved even in the absence of co-reactors such as H_2O_2. The as designed ECL biosensor showed excellent sensitivity for MCF-7 exosomes detection, and it can also be applied to serum samples analysis, which provide a powerful tool for the evaluation of exosomes surface protein expression and the physiological functions of exosomes in metabolic processes.

2. Experimental

2.1. Materials and reagents

The sequence of the capturing aptamer1 for EpCAM on exosomes was 5′-NH_2-TTTTTTCACTACAGAGGTTGCGTCTGTCCCACGTTGTCATGGGGGGTTGGCCTG, the probe aptamer2 for CD63 on exosomes was 5′-COOH-TTTTTTCACCCCACCTCGCTCCCGTGACACTAATGCTA and the random aptamer was 5′-NH_2-TTTTTTACACATTACAGGGGTTCGGTCTGGAAAGCAGTTACTGTC CCCTTGGGT, all of above aptamer were obtained from Shanghai Sangon Biological Engineering Technology & Services Co., Ltd. Ti_3AlC_2 (98%) was purchased from Forsman Scientific Co., Ltd. (Beijing, China). Poly (N-isopropylacrylamide), carboxylic acid terminated (PNIPAM, Mn = 2000) and luminol were purchased from Sigma-Aldrich. $HAuCl_4{\cdot}3H_2O$ (48%, w/w) was obtained from Shanghai Reagent (Shanghai, China). Polyethyleneimine (PEI, MW = 70000) purchased from Shanghai Macklin Biological Technology Co., Ltd. 1-(3-(dimethyl-amino)propyl)-3-ethylcarbodiimidehydrochloride (EDC), and N-hydroxysuccinimide sodium salt (NHS), Phosphate buffer solutions (PBS) were prepared with $Na_2HPO_4{\cdot}12H_2O$ and $NaH_2PO_4{\cdot}2H_2O$, Ethylenediamine (EDA) and Dimethyl sulfoxide (DMSO) were obtained from Beijing Chemical Co. (Beijing, China). The glassy carbon electrode (GCE) was purchased from CH Instruments, INC.

2.2. Apparatus and characterization

The scanning electron microscopy (SEM) image was obtained using a JSM-7401 field emission SEM system (JEOL, Japan). UV–vis spectra were collected with a UV-3900 spectrophotometer (Hitachi, Japan). Fourier transform infrared (FT-IR) spectra were obtained on a PerkinElmer Spectrum GX spectrometer (PerkinElmer Co., Waltham, MA). The X-ray diffraction (XRD) patterns were collected using a D8 Advance (Bruker) X-ray diffractometer with Cu Kα radiation (λ = 1.5418 Å). The atomic force microscopy (AFM) was conducted on Dimension Icon (Bruker Nano Inc, USA). The cyclic voltammetry (CV) was obtained on a CHI660b instrument (CH Instrument Co., USA). Electrochemical impedance spectroscopy (EIS) was conducted on a PARSTAT 2273 potentiostat/galvanostat (Advanced Measurement Technology Inc., USA) by applying an AC voltage amplitude of 5 mV in a frequency range from 0.1 Hz to 100 kHz in a 5 mM $K_3[Fe(CN)_6]/K_4[Fe(CN)_6]$ as the redox probe solution with 0.5 M KCl. The ECL measurements were carried out on an MPI-B multifunctional electrochemical analytical system (Xi'an Remex Analytical Instrument Ltd. Co., China). The voltage of the photomultiplier tube (PMT) was maintained at 600 V.

2.3. The preparation of gold nanoparticles (AuNPs), Ti_3C_2 MXenes (MXenes) and MXenes-Aptamer2 (MXenes-Apt2) Nanoprobe

The AuNPs were fabricated as previously reported (Chen et al., 2014). In briefly, 100 mL of 0.01% (w/v) $HAuCl_4$ solution was boiled with vigorous stirring, then 0.588 mL of 0.2 mol L^{-1} trisodium citrate solution was quickly added into the boiling solution. The solution turned deep red, indicating the formation of AuNPs. The final AuNPs colloid solution was stored at 4 °C for the next experiments. As shown in Fig. S2A, the UV–Vis spectrum of AuNPs showed a strong adsorption at 520 nm, which is the corresponding absorption of AuNPs and indicated the formation of around 20 nm AuNPs.

Ti_3AlC_2 (1.0 g) powders were immersed in 15 mL of 48% HF, and was stirred for 24 h at 45 °C. Then, the suspensions were centrifuged to separate solids from the supernatant. After that the solid products were washed until the pH of the suspension reached 6, and were dried at room temperature. The solid products were then immersed in 1 mL DMSO for 24 h under stirring at room temperature. After centrifugation, the sediment was retained and washed with DI water. Finally, the dispersed solution was centrifuged at 3500 rpm for 60 min, and the supernatant was retained and stored at 4 °C for next experiments.

0.005 g mL^{-1} PEI, 3 mL MXenes and 2 mL DI water were mixed, and was slowly stirred for 1 h at room temperature. Then, the suspensions were centrifuged to separate solids from the supernatant. After centrifugation, the sediment was retained and added with DI water to gain MXenes-PEI. In addition, the Apt2 (1 μM) was activated by EDC (400 mM) and NHS (100 mM) for 1 h at 37 °C. After that, 200 μL MXenes-PEI solution was added into the Apt2 mixture solution for 1 h at 37 °C. Finally, the dispersed solution was centrifuged at 12000 rpm for 10 min, then the sediment was retained and added with DI water to gain MXenes-Apt2 nanoprobe for next experiments.

2.4. Cell culture, exosomes extraction and counting

Melanoma cells line (B16 cells), breast cancer cell line (MCF-7 cells), and human liver cancer cell line (HepG2 cells) were cultured in DMEM supplemented with 10% FBS and 1% penicillin/streptomycin in a humidified atmosphere with 5% CO_2 at 37 °C. The cells were cultured for 48 h to reach 70% cell confluence and the supernatant containing exosomes were harvested. Subsequently, the exosomes were isolated from the above cell culture medium supernatant, and were stored at 4 °C. The collected supernatant (300 mL) was centrifuged at 500 g for 10 min, and then the acquired supernatant was continuously centrifuged at 2000 g for 20 min. After that, the supernatant was subjected to membrane filtration (0.8 μm pore size), followed by centrifugation at 10000 g for 90 min and centrifugal filtration (50 kDa) at 3000 g for 15 min to concentrate the solution to 40 mL. The obtained solution was then treated by a subsequent membrane filtration (0.2 μm pore size), and an ultracentrifugation at 100000 g for 90 min to obtain the exosomes. The exosomes were stored at −20 °C for further use. The exosomes counting was measured by Nanoparticle Tracking Analysis (NTA) technique, which can determine the purity of the separation and the size distribution of the obtained exosomes. The results showed that the mode size of exosomes is about 170 nm and the concentration of exosomes is approximately 2.4×10^8 particles/mL (Fig. S1) (Liu et al., 2017a, 2017b). The exosomes were diluted to the desired concentration to conduct the detection experiments. The measurements were performed at 20 °C.

2.5. Biosensor fabrication

The glassy carbon electrode (GCE; diameter of 3 mm) was processed with 0.3 and 0.05 μM α-Al_2O_3 powder and rinsed ultrasonically with ethanol and DI water, respectively, finally it was dried with N_2. Drop 6 μL of AuNPs solution on pretreated GCE to form AuNPs/GCE, then, the AuNPs/GCE electrode was immersed in 120 μL of mixture solution containing 2 mg mL^{-1} EDA, 400 mM EDC and 100 mM NHS at 37 °C for 2 h. 1 mg mL^{-1} PNIPAM was activated by 400 mM EDC and 100 mM NHS at 37 °C for 1 h. Then, the AuNPs/GCE was immersed in the activated solution of the PNIPAM at room temperature for 1 h to form PNIPAM-AuNPs/GCE. The immobilization of aptamer1 (Apt1) was finished by incubating the PNIPAM-AuNPs/GCE in 40 μL of 1 μM Apt1 solution at 37 °C for 2 h. MCF-7 exosomes were captured by immersing the above electrode in 100 μL MCF-7 exosomes suspension at certain concentrations. Finally, the exosomes captured electrode (exosomes/Apt1/PNIPAM-AuNPs/GCE) was carefully rinsed with DI water, and was incubated with 60 μL of the MXenes-Apt2 nanoprobe for 2 h at 37 °C. Finally, the MXenes-Apt2 nanoprobe modified electrode (MXenes-Apt2/exosomes/Apt1/PNIPAM-AuNPs/GCE) was carefully rinsed with DI water and used for subsequent ECL characterization.

3. Results and discussion

3.1. ECL of luminol on MXenes-modified electrode

The ECL behavior of luminol on MXenes/GCE electrode was studied. As shown in Fig. 1, the ECL responses on the MXenes/GCE electrode (curve b) were obviously larger than that on bare GCE electrode (curve a), which confirmed that MXenes can enhance ECL of luminol. While the MXenes/GCE electrode was immersed in a nitrogen-filled 100 μM luminol, the ECL signal was sharply decreased (curve c). In addition, superoxide dismutase (SOD) is a traditional O_2• capture, it was added to the air saturation solution to detect impact of O_2•. As shown in Fig. 1 (curve d), the ECL signal decreased significantly in the presence of SOD. These results suggest that oxygen was critical for the ECL behavior of luminol on the MXenes/GCE electrodes. Therefore, we put forward that the ECL response of luminol could be attributed to the excellent electrocatalytic properties of MXenes, the electrocatalytic properties could promote the reduction of O_2 in a solution dissolved with trace oxygen. The resulting reactive oxygen species such as O_2• could further oxidize luminol to form 3-aminophthalate and eventually light was emitted. Since the ECL peak of luminol on bare GCE electrode and MXenes/GCE was located at ca. 0.6 V (Fig. S6), the potential range for ECL detection was chosen in the range of 0–0.6 V. In addition, we found that the ECL responses on the MXenes/GCE electrode presented excellent stability during the experiment (as shown in Fig. S7). These results mean that highly sensitive ECL biosensor can be obtained based on the ECL behavior of luminol on GCE electrode modified with MXenes.

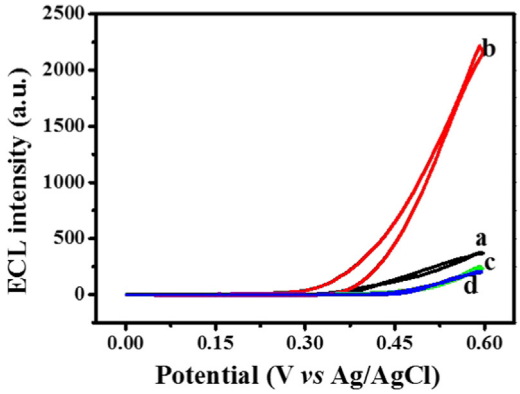

Fig. 1. The ECL response of the bare GCE electrode in 100 μM luminol (a), MXenes/GCE electrode in 100 μM luminol (curve a) before (curve b) and after (curve c) being saturated with nitrogen and performed in the electrolyte containing 35 U of SOD without deaeration (curve d).

3.2. MXenes catalyzed highly efficient ECL biosensor for sensitive exosomes detection

Scheme 1 shows the construction of the ECL biosensor based on MXenes-Apt2 nanoprobe for detection of exosomes. PNIPAM-AuNPs composite layer was first coated on the GCE surface to provide more carboxyl for immobilizing Apt1, the Apt1 can recognize the EpCAM on the surface of exosomes with high affinity. After exosomes were captured, the electrodes were incubated in the solution with MXenes-Apt2 nanoprobe forming a sandwich type system based on the highly specific recognition between Apt2 and exosomes. The ECL signal of the MXenes-Apt2/exosomes/Apt1/PNIPAM-AuNPs/GCE in luminol solution was recorded, which was related to the numbers of exosomes. In addition, MXenes nanosheets can significantly improve the ECL signal of luminol in the absence of co-reactors such as H_2O_2, and the enhanced effect of MXenes for the ECL of luminol is greatly reduced in the nitrogen-filled luminol and in the presence of SOD (Fig. 1). Therefore, MXenes can catalyze the ECL of luminol in the presence of oxygen. Here, the MXenes nanosheets are not only used to catalyze the ECL process of luminol but also acted as a carrier to provide the large surface area that it can load a mass of Apt2 for exosomes capture. Moreover, owing to its excellent electron transfer ability, the MXenes nanosheets also improve the electron transfer at the electrode interface, thus improving the sensitivity of as-designed ECL biosensor for exosomes detection.

3.3. Characterization of Ti_3C_2 MXenes and MXenes–Apt2 nanoprobe

The successful synthesis of Ti_3C_2 MXenes was confirmed by XRD, SEM and TEM patterns (Fig. S2B-F). Fig. S2B shows the XRD pattern of Ti_3AlC_2 before (a) and after HF etching (b). The disappearance of the main peak (104) and the offset of the (002) peak of Ti_3AlC_2 reflected good etching effect (Ghidiu et al., 2014), which indicated that Ti_3C_2 MXenes have been successfully prepared. This result can also be proven by SEM images, Fig. S2C shows particles shape of the solid dense MXene. The Ti_3C_2Tx MXenes possessed a layered structure in Fig. S2D.

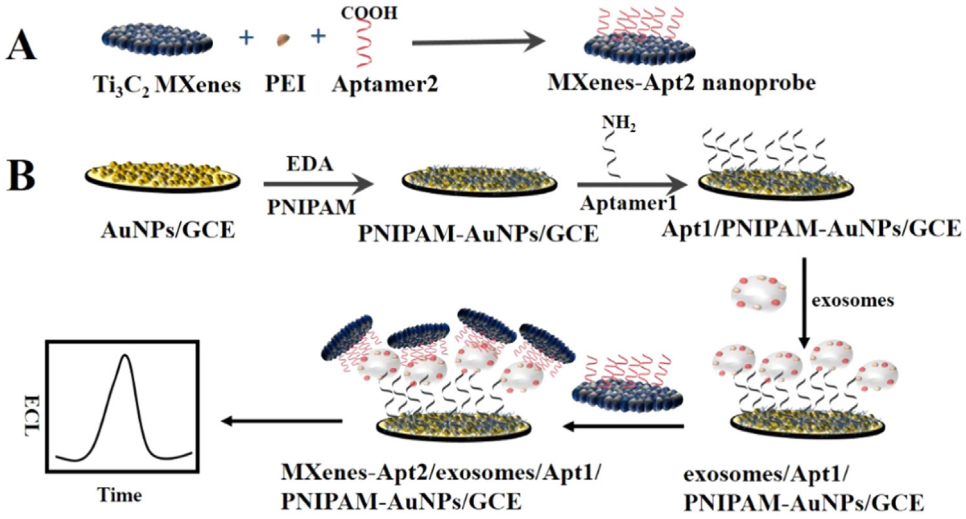

Scheme 1. The principle of the ECL biosensor for exosomes activity detection signal amplification strategy.

After exfoliation, the Ti_3C_2 MXenes were obtained as nanosheets (Fig. S2E). The AFM characterization presented that the thickness of nanosheets were about 1.85 nm, indicating that they are mainly comprised of single layer (Fig. S2F). The obtained dark-green MXenes exhibited good dispersion in aqueous solutions and the average particle size of the MXenes was centered at around 1 μm as shown in Fig. S3.

The formation of MXenes-Apt2 was characterized by the FT-IR spectra and Zeta potential. Fig. S4A showed the FT-IR spectra of the PEI (curve c), MXenes (curve b), and PEI-conjugated MXenes (MXenes-PEI) (curve a). The peak at 1630 cm^{-1} in curve c corresponded to the N–H bending vibration in PEI. The peaks at ~1389 and ~665 cm^{-1} in curve b corresponded to the O-H and Ti-O stretching vibration in MXenes, respectively. Curve a in Fig. S4A presented the FT-IR spectrum of the MXenes-PEI composite. The peaks of the N–H, O-H and Ti-O could also be observed in curve a. These facts confirm that PEI polymer was conjugated onto the MXenes successfully. The Zeta potential of MXenes, MXenes-PEI, PEI and MXenes-Apt2 were shown in Fig. S4B, the MXenes present negative Zeta potential, and the PEI polymer exhibit positive Zeta potential, after the modification of PEI, the MXenes-PEI composite manifests a high positive Zeta potential. MXenes-PEI and Apt2 were covalently combined to form the MXenes-Apt2 nanoprobe. Since Apt2 was negatively charged, the MXenes-Apt2 nanoprobe presented negative Zeta potential (Fig. S4B). These results indicate that the Apt2 was modified on the MXenes-PEI composite successfully.

3.4. Electrochemical characterizations of the biosensor

CV and EIS are used to prove the modified electrode assembly process gradually. Fig. 2A showed the CV curves of the modified GCE using Fe (CN) $_6^{4-/3-}$ as electroactive probes. The reversible redox peaks of the AuNPs/GCE were observed in (curve b). After the modification of PNIPAM, the peak currents of the electrode increased (curve c), attributing to the large surface and the excellent electrical conductivity of PNIPAM-AuNPs. When the Apt1 was modified onto the above electrode, the amperometric signal was slight decrease (curve d). The peak currents in CV were decreased rapidly after capture of MCF-7 exosomes (curve e). These results are due to the electronically inert feature of Apt1 and exosomes that hinder the electron transfer and mass transfer of Fe (CN) $_6^{4-/3-}$ ions on the electrode surface. Finally, the biosensor was incubated with the MXenes-Apt2 nanoprobe, the peak currents were increased obviously, owing to the large specific surface and good conductivity of the nanoprobe (curve f). Fig. 2B displayed the EIS curves. The Nyquist plot includes a semicircle part at a higher frequency range and a straight linear part at a lower frequency range.

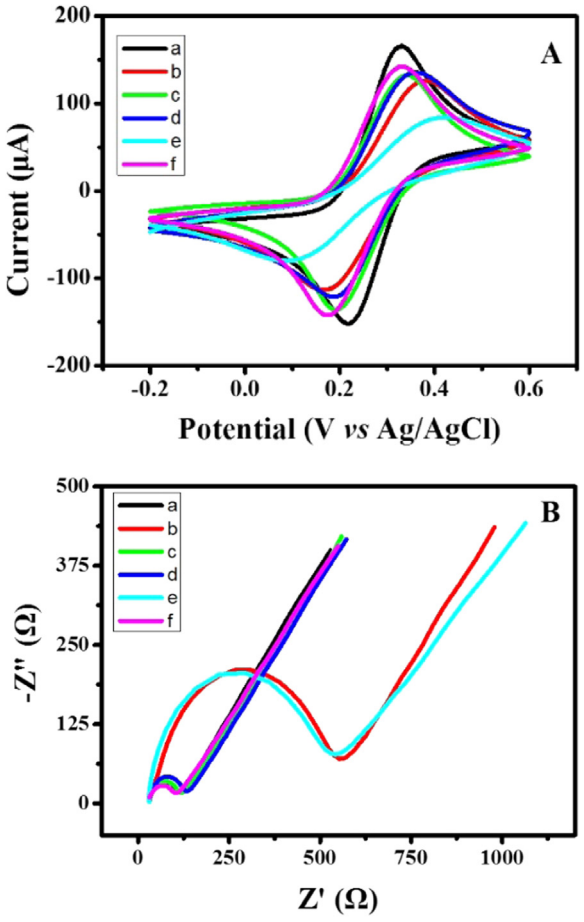

Fig. 2. Cyclic voltammograms (A) and electrochemical impedance spectra (B) of bare GCE (a) AuNPs/GCE (b) PNIPAM-AuNPs/GCE (c) Apt1/PNIPAM-AuNPs/GCE (d) exosomes/Apt1/PNIPAM-AuNPs/GCE (e) and MXenes-Apt2/exosomes/Apt 1/PNIPAM-AuNPs/GCE (f) in 5 mM $[Fe(CN)_6]^{3-/4-}$ containg 0.1 M KCl solution (pH 7.0). The scan rate is 100 mV s^{-1}. The impedance spectra frequency is 0.1–10^5 Hz.

The diameter of the semicircle equals the electron transfer resistance (Ret) at the electrode interface. The PNIPAM-AuNPs/GCE (curve c) showed lower Ret than AuNPs/GCE (curve b). After that, the Apt1 (curve d) and the exosomes (curve e) were sequentially assembled, the

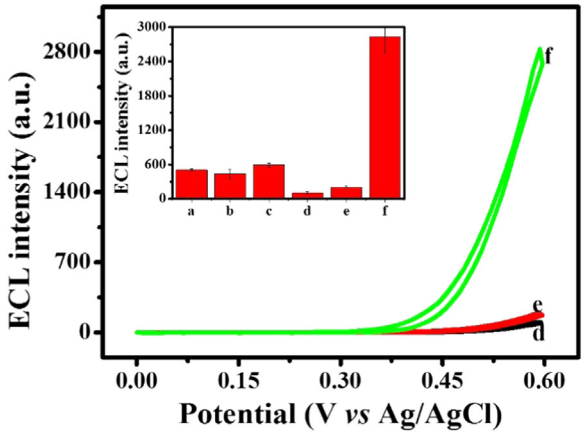

Fig. 3. ECL intensity-potential behavior of bare GCE electrode (a), AuNPs/GCE (b) PNIPAM-AuNPs/GCE (c), Apt1/PNIPAM-AuNPs/GCE (d), exosomes/Apt1/PNIPAM-AuNPs/GCE (e) and MXenes-Apt2/exosomes/Apt1 /PNIPAM-AuNPs/GCE (f) in 100 μM luminol. The scan rate is 100 mV s^{-1}. The PMT voltage is 600 V. The potential is 0 ~ 0.6 V (vs Ag/AgCl). The concentration of MCF-7 exosomes is 1 × 10^5 particles μL^{-1}.

diameter of the semicircle increases sequentially. Finally, the electrode showed the lower Ret when the MXenes-Apt2 nanoprobe were incubated. These results have same trend with the outcomes in CVs, proving successful assembly biosensor.

3.5. ECL behaviors of the biosensor

In this strategy, the ECL responses from MXenes-Apt2 nanoprobe was closely related with the exosomes captured on the electrode. In addition, the MXenes-Apt2 nanoprobe was adsorbed on the exosomes surface based on the specific affinity between the Apt2 and exosomes. Therefore, the ECL responses from MXenes-Apt2 nanoprobe could be used to detect exosomes. Series of control experiments were conducted with ECL measurements to verify feasibility of this ECL sensor. As shown in Fig. 3, bare GCE electrode, AuNPs/GCE and PNIPAM-AuNPs/GCE without incubating exosomes and Apt1 showed slight ECL emission (curves a, b, c). In addition, the Apt1/PNIPAM-AuNPs/GCE and exosomes/Apt1/PNIPAM-AuNPs/GCE without MXenes-Apt2 nanoprobe immobilization showed lower ECL signals, owing to the electron-transfer inhibition on the electrode interface by the Apt1 and exosomes (curves d, e). In contrast, biosensor formed well under all procedures showed strong ECL intensity (curve f). These results indicate that Apt2 had a strong affinity with exosomes and the enhancement of the ECL signal could be ascribed to the excellent electrocatalytic ability and electron-transport ability of MXenes-Apt2 nanoprobe. Therefore, the proposed biosensor was sensitive and feasible.

3.6. Optimization of the experimental conditions

The effect of exosomes incubation temperature and time, the concentrations of Apt1 and luminol for performances of the ECL biosensor were tested. The optimal exosomes incubation temperature was 37 °C as shown in Fig. S5a. As a result, the exosomes incubation temperature was 37 °C was used in the following experiments. The incubation time for exosomes is crucial for the ECL sensing. It can be seen that the ECL intensity of the biosensor improved with increasing exosomes incubation time and then reached a maximum at 120 min (Fig. S5b). The concentrations of Apt1 also influenced the ECL performance of the biosensor, the ECL intensity as a function of Apt1 concentrations was shown in Fig. S5c, the ECL intensity at the 1 μM Apt1 was greater than the ECL intensities of 0.8 μM and 1.2 μM Apt1. Meanwhile, as shown in Fig. S5d, the ECL intensity promoted with increasing luminol concentrations, then reached a maximum at 100 μM. Therefore, the optimal conditions for the biosensor were 37 °C and 120 min for exosomes capture, 1 μM for Apt1 and 100 μM for luminol.

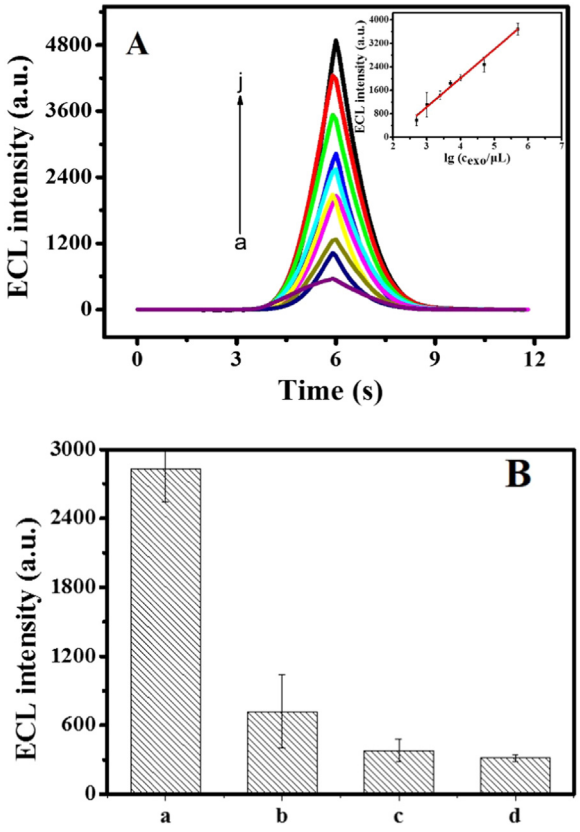

Fig. 4. (A) The ECL intensities of assay versus different MCF-7 exosomes concentrations (from a to j was 5.0 × 10^2, 1 × 10^3, 2.5 × 10^3, 5 × 10^3, 10^4, 5 × 10^4, 10^5, 5 × 10^5, 10^6, 5 × 10^6 particles μL^{-1}, respectively) in 100 μM luminol. The inset is a plot of ECL intensity vs the logarithm value of the MCF-7 exosomes concentration. The PMT voltage is 600 V. (B) ECL intensity of the MXenes-Apt2/exosomes/Apt1/PNIPAM-AuNPs/GCE electrode (a), MXenes-Apt2/Apt1/PNIPAM-AuNPs/GCE (b), Mxenes-Apt2/exosomes/PNIPAM-AuNPs/GCE electrode (c) and MXenes-Apt2/exosomes/random Apt/PNIPAM-AuNPs/GCE electrode (d) in 100 μM luminol. The PMT voltage is 600 V. The concentration of MCF-7 exosomes was 1 × 10^5 particles μL^{-1}.

3.7. Exosomes sensing of the biosensor

Under the optimal conditions, the sandwiched ECL biosensor was applied to the MCF-7 exosomes detection. Fig. 4A showed the ECL signal intensities of luminol at different concentrations of the MCF-7 exosomes. It can be seen that the ECL signal intensities enhanced with the increased exosomes concentrations. A good linear relationship between the ECL intensity and the logarithm of the exosomes concentration was obtained in the range from 5 × 10^2 to 5 × 10^6 particles μL^{-1}. The linear regression equation is I = 991.1461 log [C_{exo} (exo uL^{-1})] – 4929.067 with a correlation coefficient of R^2 = 0.9790 (n = 3), where I is the ECL intensity and C_{exo} is the MCF-7 exosomes concentration. The limit of detection (LOD) can be calculated based on the formula of Log (LOD) = $\frac{3\theta - b}{k}$, where θ is the background standard deviation, b is the intercept in the linear regression equation and k is the slope of the linear regression equation. The detection limit (3σ) was 125 particles μL^{-1}(signal-to-noise ratio of 3). The high sensitivity could attribute to the catalysis of MXenes-Apt2 nanoprobe. This shows that the designed ECL biosensor can be employed for highly sensitive MCF-7 exosomes detection.

In addition, the specificity of the ECL biosensor between Apt1 and exosomes, and between MXenes-Apt2 nanoprobe and exosomes were

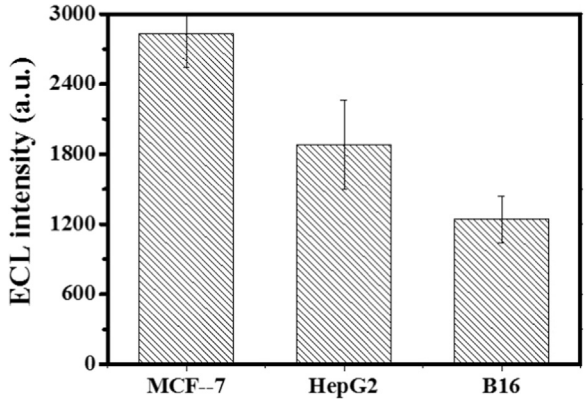

Fig. 5. The ECL responses of the biosensor to the exosomes from different cells lines. The concentration of exosomes was 1×10^5 particles μL^{-1}.

also studied (Fig. 4B). The MXenes-Apt2/exosomes/Apt1/PNIPAM-AuNPs/GCE (a) showed the larger ECL signal than the MXenes-Apt2/Apt1/PNIPAM-AuNPs/GCE (b), this is because (a) was incubated in the MCF-7 exosomes solution and the exosomes were captured on the electrode, so more MXenes-Apt2 nanoprobe was modified on the electrode to generate larger ECL signal. This result means that there was specificity between MXenes-Apt2 nanoprobe and exosomes. At the same time, curve a showed a larger ECL signal than curve c and curve d. It could be ascribed to that Apt1 was modified on the electrode to capture more exosomes, and then more MXenes-Apt2 nanoprobe was adsorbed onto the exosomes. Thus, the ECL signal increased. These results demonstrated the high specificity between Apt1 and exosomes.

The reproducibility of the ECL biosensor was also studied. The relative standard deviation (RSD) of this ECL biosensor was evaluated by independently testing each sample in triplicate. This result showed that the RSD of this ECL biosensor for 10^4 and 10^5 particles μL^{-1} of MCF-7 exosomes were 3.2% and 4.5% respectively, the as-designed ECL biosensor showed good reproducibility. At the same time, Fig. S8 showed that the ECL signal of this biosensor was stable during successive scanning, indicating that the ECL biosensor had excellent cycling stability.

3.8. Detection of exosomes activity in serum

To prove the potential of the constructed ECL biosensor in clinical applications. Different concentrations of MCF-7 exosomes added to the serum were measured by using the MXenes-based ECL biosensor. The recovery ranged from 95% to 104% was obtained and displayed in Table S1. What' more, the serum containing the mixture of normal exosomes and MCF-7 exosomes with a concentration of 5×10^3 particles μL^{-1} was also measured by using the MXenes-based ECL biosensor. The experimental result was shown in Fig. S9. Due to the complexity of the biological sample, the MXenes-Apt2/exosomes/Apt1/PNIPAM-AuNPs/GCE (a) in serum showed larger ECL signal than the MXenes-Apt2/exosomes/Apt1/PNIPAM-AuNPs/GCE (b) in serum containing normal exosomes. The above results clearly indicated that the as-prepared MXenes-based ECL biosensor can also be applied to the clinical serum sample assay.

To further prove the applicability of the ECL biosensor for exosomes detection, the as-designed ECL biosensor was incubated in the exosomes from MCF-7, HepG2 and B16 cells lines. The results were shown in Fig. 5, when the electrode was immersed in the exosomes solution from MCF-7 cell line, the largest ECL signal was observed, and the smallest ECL signals were observed in the exosomes solution from B16 cell line. Since the ECL signal is associated to the expression of EpCAM on the surface of exosomes, the results demonstrated that the highest expression of EpCAM on the exosomes from MCF-7 cell line, which was similar to that previously reported (Liu et al., 2018).

4. Conclusions

In conclusion, a novel ECL biosensor was developed based on aptamer recognition and catalytic ECL signal amplification of Ti_3C_2 MXenes nanosheets because of their large surface area, excellent conductivity and catalytic properties. Highly efficient exosomes capture on the electrode and the significantly ECL signal responses can be realized. The as prepared ECL biosensor for MCF-7 exosomes exhibited high sensitivity with a lower detection limit of 125 particles μL^{-1}, which was 100 times lower than that of conventional ELISA method. In addition, this ECL biosensor had been proven to be flexible owing to that it can be used to detect different exosomes and can be applied to exosomes detection in serum samples. This novel ECL biosensor with amplified strategy not only is helpful to the understanding of complex exosomes-related biological processes, but also can serve as a tool for explanting the physiological processes of exosomes-related diseases.

Acknowledgments

This work was financially supported by National Key Research and Development Program of China (No.2016YFA0203101), National Natural Science Foundation of China (No. 21874080, 21475071, 21622506, 21621003), Beijing Municipal Science and Technology Commission (Z171100001117135), the Taishan Scholar Program of Shandong Province (ts201511027) and the Natural Science Foundation of Shandong (2018GGX102030).

Appendix A. Supporting information

Supplementary data associated with this article can be found in the online version at doi:10.1016/j.bios.2018.10.016.

References

Bertoncello, P., Forster, R.J., 2009. Biosens. Bioelectron. 24, 3191–3200.
Chen, X., Wang, Y., Zhang, Y., Chen, Z., Liu, Y., Li, Z., Li, J., 2014. Anal. Chem. 86, 4278–4286.
Chen, Z., Liu, Y., Wang, Y., Zhao, X., Li, J., 2013. Anal. Chem. 85, 4431–4438.
Cheng, Y., Huang, Y., Lei, J., Zhang, L., Ju, H., 2014. Anal. Chem. 86, 5158–5163.
Chiu, Y.J., Cai, W., Shih, Y.R., Lian, I., Lo, Y.H., 2016. Small 12, 3658–3666.
Dall'Agnese, Y., Taberna, P.L., Gogotsi, Y., Simon, P., 2015. J. Phys. Chem. Lett. 6, 2305–2309.
Dong, Y., Mallineni, S.S.K., Maleski, K., Behlow, H., Mochalin, V.N., Rao, A.M., Yuan, W., Cheng, L., Wu, H., Zhang, Y., Lv, S., Guo, X., 2018. Chem. Commun. 54, 2755–2758.
Dong, Y.P., Chen, G., Zhou, Y., Zhu, J.J., 2016a. Anal. Chem. 88, 1922–1929.
Dong, Y.P., Zhou, Y., Wang, J., Zhu, J.J., 2016b. Anal. Chem. 88, 5469–5475.
Dragovic, R.A., Gardiner, C., Brooks, A.S., Tannetta, D.S., Ferguson, D.J., Hole, P., Carr, B., Redman, C.W., Harris, A.L., Dobson, P.J., Harrison, P., Sargent, I.L., 2011. Nanomedicine 7, 780–788.
Fang, Y., Yang, X., Chen, T., Xu, G., Liu, M., Liu, J., Xu, Y., 2018. Sens. Actuators B-Chem. 263, 400–407.
Feng, Y., Dai, C., Lei, J., Ju, H., Cheng, Y., 2016. Anal. Chem. 88, 845–850.
Forzani, E.S., Lu, D., Leright, M.J., Aguilar, A.D., Tsow, F., Iglesias, R.A., Zhang, Q., Lu, J., Li, J., Tao, N., 2009. J. Am. Chem. Soc. 131, 1390.
Ghidiu, M., Lukatskaya, M.R., Zhao, M.Q., Gogotsi, Y., Barsoum, M.W., 2014. Nature 516, 78–81.
Gleadle, J., McNicholas, K., Li, J., Michael, M., Rojas-Canales, D., 2018. J. Am. Soc. Nephrol. 29, 1784.
He, Y., Li, J., Liu, Y., 2015. Anal. Chem. 87, 9777–9785.
Ji, X., Liu, B., Ren, X., Shi, X., Asiri, A.M., Sun, X., 2018a. ACS Sustain. Chem. Eng. 6, 4499–4503.
Ji, X., Liu, B., Ren, X., Shi, X., Asiri, A.M., Sun, X., 2018b. ACS Sustain. Chem. Eng. 6, 4499–4503.
Jiang, Y., Shi, M., Liu, Y., Wan, S., Cui, C., Zhang, L., Tan, W., 2017. Angew. Chem. Int. Ed. Engl. 56, 11916–11920.
Li, J., Hong, X., Li, D., Zhao, K., Wang, L., Wang, H.Z., Du, Z.L., Li, J.H., Bai, Y.B., Li, T.J., 2004. Chem. Commun. 15, 1740–1741.
Liang, X., Garsuch, A., Nazar, L.F., 2015. Angew. Chem. Int. Ed. 127, 3979–3983.
Liu, C., Guo, J., Tian, F., Yang, N., Yan, F., Ding, Y., Wei, J., Hu, G., Nie, G., Sun, J., 2017a. ACS Nano 11, 6968–6976.
Liu, C., Guo, J., Tian, F., Yang, N., Yan, F., Ding, Y., Wei, J., Hu, G., Nie, G., Sun, J., 2017b. ACS Nano 11, 6968–6976.
Liu, C., Yang, Y., Wu, Y., 2018. AAPS J. 20, 41.
Liu, X., Dong, M., Qi, H., Gao, Q., Zhang, C., 2016. Anal. Chem. 88, 8720–8727.
Lorencova, L., Bertok, T., Dosekova, E., Holazova, A., Paprckova, D., Vikartovska, A.,

Sasinkova, V., Filip, J., Kasak, P., Jerigova, M., Velic, D., Mahmoud, K.A., Tkac, J., 2017. Electrochim. Acta 235, 471–479.
Lorencova, L., Bertok, T., Filip, J., Jerigova, M., Velic, D., Kasak, P., Mahmoud, K.A., Tkac, J., 2018. Sens. Actuators B-Chem. 263, 360–368.
Lu, X., Wen, Z., Li, J., 2006. Biomaterials 27, 5740–5747.
Ma, X., Ma, M., Liu, D., Hao, S., Qu, F., Du, G., Asiri, A.M., Sun, X., 2017. Chemcatchem 9, 3138–3143.
Mathivanan, S., Ji, H., Simpson, R.J., 2010. J. Proteom. 73, 1907–1920.
Naguib, M., Kurtoglu, M., Presser, V., Lu, J., Niu, J., Heon, M., Hultman, L., Gogotsi, Y., Barsoum, M.W., 2011. Adv. Mater. 23, 4248–4253.
Naguib, M., Come, J., Dyatkin, B., Presser, V., Taberna, P.-L., Simon, P., Barsoum, M.W., Gogotsi, Y., 2012. Electrochem. Commun. 16, 61–64.
Naguib, M., Mochalin, V.N., Barsoum, M.W., Gogotsi, Y., 2014. Adv. Mater. 26, 992–1005.
Nilsson, J., Skog, J., Nordstrand, A., Baranov, V., Mincheva-Nilsson, L., Breakefield, X.O., Widmark, A. Br, 2009. J. Cancer 100, 1603–1607.
van der Pol, E., Coumans, F.A., Sturk, A., Nieuwland, R., van Leeuwen, T.G., 2014. Nano Lett. 14, 6195–6201.
Raposo, G., Stoorvogel, W., 2013. J. Cell. Biol. 200, 373–383.
Roberts, G.S., Yu, S., Zeng, Q., Chan, L.C., Anderson, W., Colby, A.H., Grinstaff, M.W., Reid, S., Vogel, R., 2012. Biosens. Bioelectron. 31, 17–25.
Seh, Z.W., Fredrickson, K.D., Anasori, B., Kibsgaard, J., Strickler, A.L., Lukatskaya, M.R., Gogotsi, Y., Jaramillo, T.F., Vojvodic, A., 2016. Acs. Energy Lett. 1, 589–594.
Ueda, K., Ishikawa, N., Tatsuguchi, A., Saichi, N., Fujii, R., Nakagawa, H., 2014. Sci. Rep. 4, 6232.
Valadi, H., Ekstrom, K., Bossios, A., Sjostrand, M., Lee, J.J., Lotvall, J.O., 2007. Nat. Cell. Biol. 99, 654–659.
Vlassov, A.V., Magdaleno, S., Setterquist, R., Conrad, R. Biochim, 2012. Biophys. Acta 1820, 940–948.
Wang, Y.M., Liu, J.W., Adkins, G.B., Shen, W., Trinh, M.P., Duan, L.Y., Jiang, J.H., Zhong, W., 2017. Anal. Chem. 89, 12327–12333.
Wang, S., Zhang, L., Wan, S., Cansiz, S., Cui, C., Liu, Y., Cai, R., Hong, C., Teng, I.T., Shi, M., Wu, Y., Dong, Y., Tan, W., 2017. ACS Nano 11, 3943–3949.
Wang, Y., Li, Z., Weber, T.J., Hu, D., Lin, C.-T., Li, J., Lin, Y., 2013. Anal. Chem. 85, 6775–6782.
Wang, Y., Tang, L., Li, Z., Lin, Y., Li, J., 2014. Nat. Protoc. 9, 1944–1955.
Wang, Z., Ren, X., Wang, L., Cui, G., Wang, H., Sun, X., 2018. Chem. Commun. 54, 10993–10996.
Wang, R., Wang, Z., Xiang, X., Zhang, R., Shi, X., Sun, X., 2018. Chem. Commun. 54, 10340–10342.
Wu, L., Lu, X., Dhanjai Wu, Z.S., Dong, Y., Wang, X., Zheng, S., Chen, J., 2018. Biosens. Bioelectron. 107, 69–75.
Xia, Y., Liu, M., Wang, L., Yan, A., He, W., Chen, M., Lan, J., Xu, J., Guan, L., Chen, J., 2017. Biosens. Bioelectron. 92, 8–15.
Xu, S., Liu, Y., Wang, T., Li, J., 2011. Anal. Chem. 83, 3817–3823.
Zhang, H.R., Wu, M.S., Xu, J.J., Chen, H.Y., 2014. Anal. Chem. 86, 3834–3840.
Zhang, L., Cheng, Y., Lei, J., Liu, Y., Hao, Q., Ju, H., 2013. Anal. Chem. 85, 8001–8007.
Zhang, Q., Qiao, Y., Hao, F., Zhang, L., Wu, S., Li, Y., Li, J., 2010. Chem. Eur. J. 16, 8133–8139.
Zhang, X., Lei, J., Wu, D., Zhao, X., Jing, Y., Zhou, Z., 2016. J. Mater. Chem. A. 4, 4871–4876.
Zhou, Y.G., Mohamadi, R.M., Poudineh, M., Kermanshah, L., Ahmed, S., Safaei, T.S., Stojcic, J., Nam, R.K., Sargent, E.H., Kelley, S.O., 2016. Small 12, 727–732.